This is a repository copy of *Effect of proximity-induced spin-orbit coupling in graphene mesoscopic billiards*.

White Rose Research Online URL for this paper:
https://eprints.whiterose.ac.uk/id/eprint/192980/

Version: Published Version

Article:

L. R. Barbosa, Anderson, G. S. Ramos, Jorge Gabriel and Ferreira, Aires orcid.org/0000-0001-6017-8669 (2021) Effect of proximity-induced spin-orbit coupling in graphene mesoscopic billiards. Physical Review B. L081111. ISSN: 2469-9969

https://doi.org/10.1103/PhysRevB.103.L081111

Reuse

Items deposited in White Rose Research Online are protected by copyright, with all rights reserved unless indicated otherwise. They may be downloaded and/or printed for private study, or other acts as permitted by national copyright laws. The publisher or other rights holders may allow further reproduction and re-use of the full text version. This is indicated by the licence information on the White Rose Research Online record for the item.

Takedown

If you consider content in White Rose Research Online to be in breach of UK law, please notify us by emailing eprints@whiterose.ac.uk including the URL of the record and the reason for the withdrawal request.

eprints@whiterose.ac.uk
https://eprints.whiterose.ac.uk/

PHYSICAL REVIEW B **103**, L081111 (2021)

Letter

Effect of proximity-induced spin-orbit coupling in graphene mesoscopic billiards

Anderson L. R. Barbosa,[1] Jorge Gabriel G. S. Ramos,[2] and Aires Ferreira[3]
[1]*Departamento de Física, Universidade Federal Rural de Pernambuco, 52171-900 Recife, Pernambuco, Brazil*
[2]*Departamento de Física, Universidade Federal da Paraíba, 58051-970 João Pessoa, Paraíba, Brazil*
[3]*Department of Physics and York Centre for Quantum Technologies, University of York, York YO10 5DD, United Kingdom*

(Received 27 December 2020; accepted 11 February 2021; published 24 February 2021)

van der Waals heterostructures based on two-dimensional materials have recently become a very active topic of research in spintronics, both aiming at a fundamental description of spin dephasing processes in nanostructures and as a potential element in spin-based information processing schemes. Here, we theoretically investigate the magnetoconductance of mesoscopic devices built from graphene proximity-coupled to a high spin-orbit coupling material. Through numerically exact tight-binding simulations, we show that the interfacial breaking of inversion symmetry generates robust weak antilocalization even when the $z \rightarrow -z$ symmetric spin-orbit coupling in the quantum dot dominates over the Bychkov-Rashba interaction. Our findings are interpreted in the light of random matrix theory, which links the observed behavior of quantum interference corrections to a transition from a circular-orthogonal to circular-symplectic ensemble.

DOI: 10.1103/PhysRevB.103.L081111

Atomically thin heterostructures of graphene and other van der Waals crystals are ideally suited for investigations of relativistic spin-orbit coupling (SOC) phenomena owing to their hybridized Dirac-like electronic structure and strong interplay between spin and lattice-pseudospin degrees of freedom [1–4]. This thrust of research has been focused on the demonstration of $\mathbb{Z}_2$ topological insulating phases [5–11] and gate-tunable spin-charge conversion effects in graphene with proximity-induced SOC [12–18].

Interface-induced SOC in a graphene flake is detectable by low-field magnetotransport measurements, which provide a sensitive probe of symmetry-breaking processes affecting the interference between time-reversed paths of electrons [19–24]. The strength of relativistic SOC effects can be estimated from the low-field changes in the magnetoconductance generated by the decrease in electron backscattering probability below its semiclassical value, a phenomenon known as weak antilocalization (WAL) [25–30]. For stacked honeycomb layers of graphene and transition metal dichalcogenides with trigonal prismatic phase coordination (known as the 1H phase), simple group theory considerations show that the allowed spin-orbit interactions comprise (spin-flip) Bychkov-Rashba (BR) interaction in addition to intrinsic-type (spin-preserving) SOC, which reflects the lowering of the point group symmetry, e.g., from D_{6h} to C_{3v} in graphene placed on semiconducting group VI dichalcogenides [31–35]. If the spin-orbit scattering time is short compared with the phase coherence time $\tau_{\rm so} \ll \tau_\phi$, the rotation of the electron's spin in the SOC field generates destructive interference, and WAL [rather than conventional weak localization (WL)] is observed. The WAL magnetoconductance peaks detected in graphene/group-VI dichalcogenide bilayers at low temperatures of a few kelvins have been attributed to proximity-induced SOC in the range 1–10 meV [19], i.e., several orders of magnitude larger than graphene's weak intrinsic SOC ($\lambda_{\rm KM} \approx 42$ μeV [10]). Such a remarkable enhancement of SOC effects (predicted by density functional theory calculations in Refs. [31,32]) is consistent with the strong reduction of spin lifetimes detected in Hanle-type spin precession measurements in such systems [36–39] and has enabled the unambiguous detection of inverse spin galvanic and spin Hall effects in graphene-based heterostructure at room temperature [12–18].

In this paper, inspired by this success in nanofabrication and measurement techniques, we investigate quantum coherent transport in two-dimensional open cavities with symmetry-breaking SOC. In the envisaged Dirac quantum dot made from a van der Waals metamaterial with proximity-induced SOC [Fig. 1(a)], scattering by the irregular boundaries destroys all constants of motion, and the system is expected to exhibit universal features of *quantum chaos* [40–47]. A unique fingerprint of quantum chaos is the emergence of universal conductance fluctuations (UCFs), which are insensitive to the system size and only depend on the symmetries of the random ensembles which describe the chaotic cavity [48–53]. To date, theoretical studies of graphene-based billiards have employed Dirac models with a mass term representing a sublattice-staggered on-site energy [54–57]. These early studies revealed that graphene billiards behave essentially as two copies of a "neutrino billiard" mutually coupled through intervalley scattering [54]. If the intervalley scattering time is much shorter than the Heisenberg time required to resolve individual energy levels, the coupling between valleys restores time-reversal symmetry, and the energy-level statistics are expected to follow the orthogonal symmetry class. Because the amount of valley mixing in a Dirac system can be adjusted by controlling the edge type [55], intervalley coupling provides a knob to tune

©2021 American Physical Society

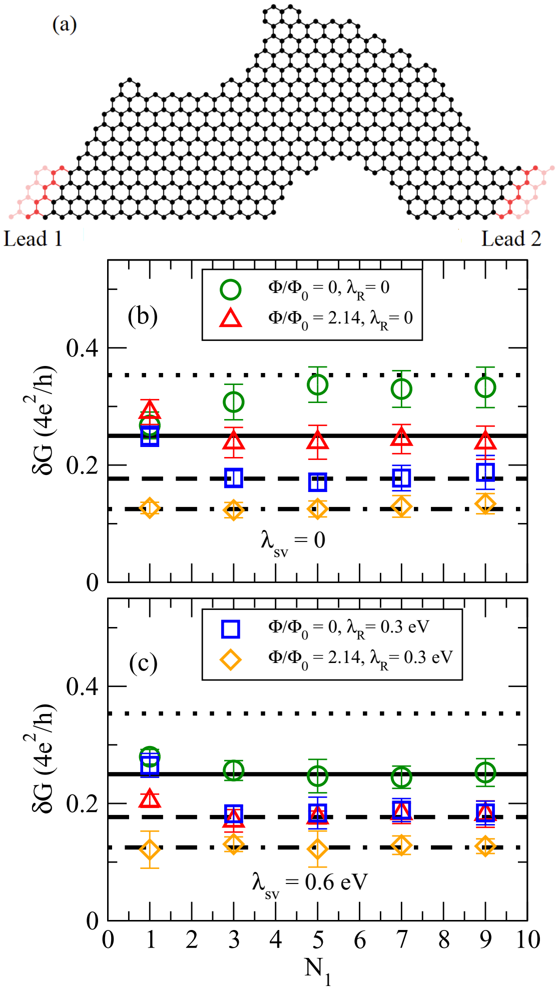

FIG. 1. (a) Dirac-Rashba billiard connected to two leads. (b) and (c) Conductance fluctuation as a function of the number of open channels for selected values of SOC and magnetic flux. Numerical data are seen to quickly converge to the predicted values in the different asymptotic limits (see Table I). Here, $\Phi_0 = h/e$ is the quantum of flux. See main text for other simulation parameters.

the symmetry class. Here, we use random matrix theory to derive a quantitative description of how proximity-induced SOC affects the statistical behavior of the conductance and its fluctuations. Our results, which extend previous studies of graphene-based chaotic billiards without SOC [53–55], are confirmed by explicit tight-binding simulations.

We consider a quantum dot weakly coupled to two electron reservoirs via ballistic point contacts, labeled 1 and 2, with N_1 and N_2 channels each [Fig. 1(a)]. The quantum dot is described by the scattering matrix, which for Dirac quasiparticles is a $4N \times 4N$ unitary matrix with $N = N_1 + N_2$, written as

$$\mathcal{S} = \begin{bmatrix} r & t' \\ t & r' \end{bmatrix}, \qquad (1)$$

where $t(t')$ and $r(r')$ are submatrices that describe transmission and reflection of Dirac quasiparticles (with spin $\sigma = \uparrow, \downarrow$ and sublattice pseudospin $\Sigma = A, B$) arriving from lead 1 (lead 2). Because of the presence of two distinct spin flavors at low energies, the $\mathcal{S}$ matrix in Eq. (1) is four times as large as that for conventional semiconductor quantum dots [45,50]. The device conductance at zero temperature is proportional to the transmission probability from lead 1 to lead 2 according to the Landauer-Büttiker formula $G = \frac{e^2}{h}\mathrm{Tr}(tt^\dagger)$. In what follows, we assume that mean dwell time is much longer than the time needed for ergodic exploration of the phase space $\tau_d \gg \tau_{\mathrm{erg}} \sim L/v$, so that the electron motion within the cavity is chaotic (here, L is the typical cavity lateral dimension, and v is the Fermi velocity). We also assume that the intervalley scattering time is short compared with the dwell time (due to strong intervalley scattering from armchair-type edges [55]), so that the conductance statistics of the open cavity are governed by the orthogonal ensemble in the absence of SOC and magnetic fields. In the universal regime of quantum transport $\tau_\phi, \tau_{\mathrm{so}} \gg \tau_{\mathrm{erg}}$, random matrix theory can be employed to calculate the conductance distribution [40]. In terms of the scattering matrix, the conductance reads as

$$G = \frac{4e^2}{h}\frac{N_1N_2}{N} - \frac{e^2}{h}\mathrm{Tr}[\mathcal{S}\mathcal{K}\mathcal{S}^\dagger\mathcal{K}], \qquad (2)$$

where $\mathcal{K}_{i,i} = N_2/N \quad (i = 1, \ldots, 4N_1)$, $\mathcal{K}_{i,i} = -N_1/N \quad (i = 4N_1 + 1, \ldots, 4N)$, and $\mathcal{K}_{ij} = 0$ for $i \neq j$. In order to find the average and variance of the conductance, it suffices to compute the average

$$\langle \mathcal{S}_{ij;\alpha\beta}(\epsilon, \vec{\mathcal{B}})\mathcal{S}^*_{i'j';\alpha'\beta'}(\epsilon, \vec{\mathcal{B}})\rangle \qquad (3)$$

in the presence of SOC and for arbitrary values of Fermi energy ϵ and magnetic field $\vec{\mathcal{B}}$ [45]. (Here, Greek indices agglutinate spin and pseudospin labels.) In what follows, we assume symmetric leads ($N_1 = N_2 = N/2$). The statistical properties of the scattering matrix $\mathcal{S}$ are calculated from random unitary matrices within the so-called "stub model"; see the Supplemental Material (SM) [58]. After a tedious but straightforward computation, the average and variance of the dimensionless conductance per sublattice and spin ($g \equiv hG/4e^2$) can be written as follows:

$$\langle g\rangle = \frac{N}{4} + \frac{1}{8}\left[\frac{1}{1+\Gamma_{\mathcal{B}}} - \frac{1}{1+\Gamma_{\mathcal{B}}+2\Gamma_{\mathrm{asy}}} - \frac{2}{1+\Gamma_{\mathcal{B}}+\Gamma_{\mathrm{asy}}+\Gamma_{\mathrm{sym}}}\right], \qquad (4)$$

$$\mathrm{var}[g] = \frac{1}{64}\sum_{j=0}^{1}\left[\frac{1}{(1+j\Gamma_{\mathcal{B}})^2} + \frac{1}{(1+j\Gamma_{\mathcal{B}}+2\Gamma_{\mathrm{asy}})^2} + \frac{2}{(1+j\Gamma_{\mathcal{B}}+\Gamma_{\mathrm{sym}}+\Gamma_{\mathrm{asy}})^2}\right], \qquad (5)$$

where $\Gamma_X = 2\tau_d/\tau_X$ with $X = \{\mathrm{sym}, \mathrm{asy}, \mathcal{B}\}$, τ_{sym} (τ_{asy}) is the spin-orbit scattering time stemming from $z \to -z$ symmetric (asymmetric) SOC [9,27,30,59,60], and $\tau_{\mathcal{B}}$ is the magnetic dephasing time [58]. Both the quantum correction to the average conductance, $\langle g_{qc}\rangle \equiv \langle g\rangle - N/4$, and the associated fluctuations, $\delta g = \sqrt{\mathrm{var}[g]}$, contain crucial information on strength and symmetry of spin-orbit effects through their dependence on Γ_{sym} and Γ_{asy}. For weak magnetic fields and weak SOC (i.e., $\tau_{\mathcal{B}}, \tau_{\mathrm{sym}}, \tau_{\mathrm{asy}} \gg \tau_d$), one finds a negative quantum correction ($g_{qc} \simeq -1/4$), which corresponds to standard WL. The behavior is markedly different in billiards where SOC

TABLE I. Ensemble transitions facilitated by strong SOC in chaotic Dirac-Rashba billiards according to random matrix theory [Eqs. (4) and (5)]. COE, CUE, and CSE refer to the standard circular ensembles (orthogonal, unitary, and symplectic, respectively). The ✓ (×) symbol indicates the presence (absence) of a given symmetry. SRS, spin rotational symmetry; TRS, time-reversal symmetry.

Limit	TRS	SRS	Strong SOC	Ensemble	$\langle g_{qc}\rangle$	δg	$\frac{\delta g_{\text{COE}}}{\delta g}$
$\tau_{\mathcal{B}}, \tau_{\text{sym}}, \tau_{\text{asy}} \gg \tau_d$ (Refs. [53,55])	✓	✓	no	COE	−0.250	0.353	1
$\tau_{\text{sym}}, \tau_{\text{asy}} \gg \tau_d \gg \tau_{\mathcal{B}}$ (Refs. [53,55])	×	✓	no	CUE	0.000	0.250	$\sqrt{2}$
$\tau_{\mathcal{B}}, \tau_{\text{asy}} \gg \tau_d \gg \tau_{\text{sym}}$	×	×	yes	CUE	0.000	0.250	$\sqrt{2}$
$\tau_{\mathcal{B}} \gg \tau_d \gg \tau_{\text{asy}}$	✓	×	yes	CSE	0.125	0.176	2
$\tau_{\text{asy}} \gg \tau_d \gg \tau_{\mathcal{B}}, \tau_{\text{sym}}$	×	×	yes		0.000	0.176	2
$\tau_d \gg \tau_{\mathcal{B}}, \tau_{\text{asy}}$	×	×	yes		0.000	0.125	$2\sqrt{2}$

acts as a symmetry-breaking perturbation. We find several regimes, depending on the relative magnitude of spin-orbit scattering times. If the electron dwell time is much greater than the spin-flip scattering time, τ_{asy}, the spin rotational invariance is broken, and the quantum correction to the average conductance becomes positive; that is, the system exhibits WAL. Using Eqs. (4) and (5), we easily find $g_{qc} \simeq 0.125$ and UCF amplitude $\delta g \simeq 0.176$. In contrast, for $\tau_{\text{asy}} \gg \tau_d \gg \tau_{\text{sym}}$, the quantum correction to the average conductance is strongly suppressed ($\langle g_{qc}\rangle \simeq 0$), and $\delta g \simeq 0.250$, which is characteristic of quantum dots with scattering matrix distributed according to the circular-unitary ensemble [40]. The effective breaking of time-reversal symmetry in this regime can be understood from the phenomenology of SOC in honeycomb layers. The spin-valley coupling (present in materials with broken sublattice symmetry, such as group-VI dichalcogenides) acts at low energies as a valley-Zeeman field, thus mimicking a magnetic field [61]. We compiled our results in Table I.

To validate the random matrix theory predictions, we perform numerically exact real-space simulations of the magnetoconductance of the chaotic system. For simplicity, we consider a graphene nanostructure proximity coupled to a high-SOC semiconductor; see Fig. 1(a). The Hamiltonian of the quantum dot can be expressed as $H = H_g + H_{\text{SO}}$, where H_g describes the usual nearest-neighbor hopping between p_z orbitals and $H_{\text{SO}} = H_{\text{sym}} + H_{\text{asy}}$ captures the proximity-induced SOC [32,34,62]. (We neglect the intrinsic Kane-Mele SOC of graphene [10], which is too weak to cause any significant perturbation to the quantum dot.) In terms of annihilation (creation) operators $c_{i,\sigma}$ ($c^{\dagger}_{i,\sigma}$) that remove (add) electrons to site i with spin $\sigma =\uparrow, \downarrow$, the terms H_g, H_{sym}, and H_{asy} read as

$$H_g = -\sum_{\langle i,j\rangle,\sigma} t^{ij} c^{\dagger}_{i,\sigma} c_{j,\sigma}, \tag{6}$$

$$H_{\text{sym}} = -\sum_{\langle\langle i,j\rangle\rangle,\sigma} \frac{\imath \lambda^{ij}_{\text{sym}}}{3\sqrt{3}} c^{\dagger}_{i,\sigma} [s_z]_{\sigma\sigma} c_{j,\sigma}, \tag{7}$$

$$H_{\text{asy}} = -\sum_{\langle i,j\rangle,\sigma,\sigma'} \frac{2\imath \lambda^{ij}_{\text{asy}}}{3} c^{\dagger}_{i,\sigma} ([\mathbf{s}]_{\sigma\sigma'} \times \hat{\mathbf{r}}_{ij})_z c_{j,\sigma'}, \tag{8}$$

where the indices i and j run over all lattice sites, $\langle\cdots\rangle$ ($\langle\langle\cdots\rangle\rangle$) denotes a sum over nearest-neighbor (next-nearest-neighbor) sites, $\hat{\mathbf{r}}_{ij}$ is the unit vector along the line segment connecting sites i and j, and $t^{ij} = te^{\imath\phi_{ij}}$, $\lambda^{ij}_{\text{asy}} = \lambda_{\text{BR}} e^{\imath\phi_{ij}}$, and $\lambda^{ij}_{\text{sym}} = \lambda_{\text{sv}} \delta_i \nu_{ij} e^{\imath\phi_{ij}}$ are Peierls's substitution modified hopping integrals with phases $\phi_{ij} = (e/\hbar)\int_{\mathbf{r}_i}^{\mathbf{r}_j} \mathbf{A}\cdot d\mathbf{r}$. Here, λ_{sv} (λ_{BR}) is the spin-valley (BR) coupling strength, and $\mathbf{A} = -B_{\perp}\hat{\mathbf{y}}$ is the magnetic vector potential in the Landau gauge. Furthermore, the ν_{ij} are signs that equal ± 1 if the electron hops clockwise (anticlockwise) to a next-nearest-neighbor site within a given hexagonal plaquette and $\delta_i = \pm 1$ distinguishes between the sublattices A (B) [9,33].

The billiard is constructed by cutting a half stadium connected to two identical leads out of a graphene sheet [54,55]. To break the left-right symmetry, we cut out circular segments at the top left and bottom right in a way that the graphene lattices are terminated abruptly [see Fig. 1(a)]. Before attempting to confirm the predicted statistical behavior of the conductance, we verify that the simulated dots support the universal quantum transport regime, $\tau_d \gg \tau_{\text{erg}}$. To estimate the dwell time, we determine the spectrum of closed cavities with an area $\mathcal{A} \approx 1.2 \times 10^3$ nm^2 (containing around 10^5 energy levels). The calculated mean level spacing (Δ) ranges from 0.2 to 0.4 meV, depending on the specific SOC parameter values; for additional details, see the SM [58]. This translates into dwell times ($\tau_d \approx \pi\hbar/N\Delta$) on the order of $\approx 10/N$ ps. Meanwhile, the electron transit time in the graphene dot is simply $\tau_{\text{erg}} \approx \sqrt{\mathcal{A}}/v$, where $v = 3at/2\hbar \approx 10^6$ m/s (assuming a typical hopping integral $t = 2.8$ eV and a lattice constant a of 0.25 nm). As a result, $\tau_d/\tau_{\text{erg}} \gg 1$ is always satisfied for typical ballistic point contacts with a small number of open channels $N \approx 1$–10.

For our numerical study, we use the recursive Green's function formalism [63–65] as implemented in the KWANT code [66]. From the earlier theoretical analysis, the spin-orbit effects are expected to influence the statistical behavior of the conductance whenever the spin-orbit scattering time, $\tau_{\text{so}} = (\tau^{-1}_{\text{asy}} + \tau^{-1}_{\text{sym}})^{-1}$, is short compared with the cavity dwell time. The conductance fluctuation δg is shown in Figs. 1(b) and 1(c) for selected parameters. In the absence of SOC, the fluctuations are consistent with the circular-orthogonal ensemble ($\delta g \simeq 0.35$) at zero field and with the circular-unitary ensemble ($\delta g \simeq 0.25$) for a magnetic flux Φ on the order of the quantum of flux [54]. After the proximity-induced SOC is turned on, the statistical properties of the quantum dot are seen to critically depend on the relative magnitude of the spin-orbit effects in complete accord with our prediction [Eqs. (4) and (5)]. A transition to the circular-symplectic ensemble ($\delta g \simeq 0.176$) is observed for sufficiently strong BR coupling in the low-field regime ($\tau_d \gg \tau_{\mathcal{B}}$). This behavior is

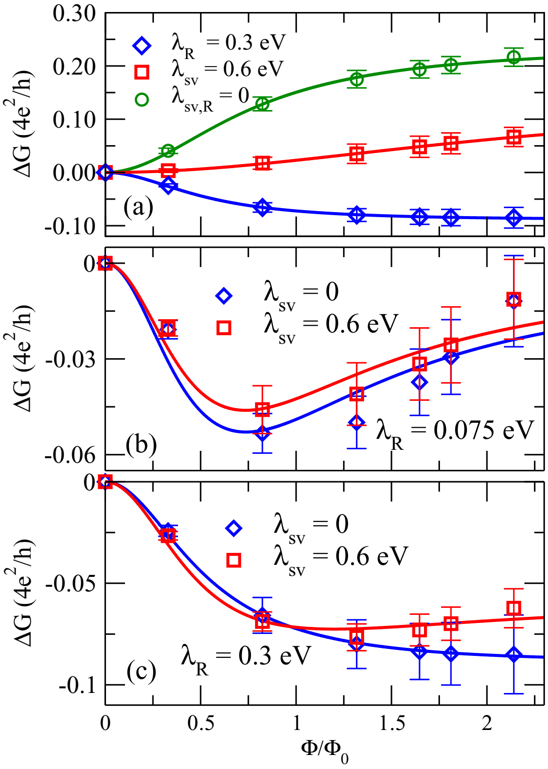

FIG. 2. (a)–(c) Average magnetoconductance as a function of the magnetic flux obtained numerically for selected SOC parameters. Solid lines are fits to Eq. (4) [58]. Data points are calculated using 20 chaotic samples averaged over the Fermi energy window [0.45,1.50] eV. Here, $\Phi_0 = h/e$ is the quantum of flux.

robust against the presence of symmetric-type SOC as long as the BR effect remains as a strong perturbation ($\tau_{\text{asy}} \ll \tau_d$). Moreover, in quantum dots with weak BR effect and strong spin-valley coupling, time-reversal symmetry is effectively broken, and as a result, the conductance fluctuation approaches the circular-unitary ensemble prediction at zero field ($\delta g \simeq 0.250$). Interestingly, the combined effect of a strong spin-valley coupling and a high magnetic field reduces the conductance fluctuation down to $\delta g \simeq 0.125$, which is lower than the UCF value in any of the Wigner-Dyson ensembles. The orthogonal to unitary or symplectic ensemble transitions facilitated by SOC and the associated statistical properties are summarized in Table I. It is important to note that due to the small quantum dot size in the simulations, the ensemble transitions are observed at rather large SOC values (≈0.1 eV). On the other hand, the experimentally achievable proximity-induced SOC energy scales are more modest (in graphene on a group-VI dichalcogenide monolayer, these range from 0.1 to 10 meV depending on the high-SOC material used and the quality of the interface [31–34]). Hence the experimental validation of our findings would require dots of substantially larger dimensions to ensure $\tau_{\text{so}} \ll \tau_d$.

Now we turn to the magnetotransport fingerprints of proximity-induced SOC. In Fig. 2, we show the calculated magnetoconductance $\Delta G(B_\perp) = \langle G(B_\perp) - G(0)\rangle$. The negative signal (WAL) observed in all simulated quantum dots with sizable BR coupling provides a clear signature of the orthogonal-to-symplectic ensemble transition. We note that this is a direct numerical evaluation of conductance WAL corrections in a chaotic billiard. In accord with the theory [cf. Eq. (4)], the BR-coupling-induced negative quantum correction is seen to be robust to the presence of symmetric SOC [see Figs. 2(b) and 2(c)]. The special role played by the spin-valley coupling in quantum dots with weak or vanishing BR effect ($\tau_{\text{asy}} \gg \tau_d$) is also borne out by the simulations. Indeed, the simulation with $\lambda_{\text{BR}} = 0$ and $\lambda_{\text{sv}} = 0.6$ eV shows a clear suppression of quantum interference effects due to spin-valley coupling since, as discussed earlier, the latter acts on the ballistic electrons as a valley-Zeeman field. The underlying spin-orbit scattering times can be estimated by fitting the numerical data to Eq. (4). We find τ_{so} to be on the order of 1 ps, which puts the simulated devices within the universal regime where the theory is expected to be accurate; see the SM for additional details [58]. We note in passing that in the absence of SOC, the magnetoconductance can be accurately fitted to the well-known expression $\Delta G/(4e^2/h) = \mathcal{G}(1 + \frac{\tau_{\mathcal{B}}}{2\tau_d})^{-1}$ [67] with $\mathcal{G} = 0.23$, in excellent agreement with the random matrix theory prediction ($\mathcal{G}_{\text{RMT}} = 0.22$).

To put our predictions into context, we first note that diffusive WAL behavior in (nonchaotic) graphene devices with interface-induced SOC is now well established [19–24,27,30]. Transition metal dichalcogenides represent a broad family of high-SOC layered materials, which can be used to fabricate the envisaged chaotic Dirac-Rashba billiard characterized by competing spin-orbit effects with different symmetries. According to our findings, chaotic billiards built from graphene-based heterostructures can display robust signatures of WAL in the universal regime of quantum transport provided that the asymmetric spin-orbit scattering time is shorter than the dwell time of the cavity. We expect that such a condition can be achieved by fabricating mesoscopic quantum dots with linear size approaching the typical (bulk) mean free paths. Electronic transport measurements on submicrometer graphene quantum dots have been recently reported [68–71], which gives us extra confidence that the predictions in this paper can be put to the test in the near future.

In summary, we have used random matrix theory to investigate the statistical behavior of the average conductance and its universal fluctuations in chaotic graphene-based billiards with proximity-induced SOC. Our study, supported by real-space quantum transport calculations, shows that the proximity-induced SOC strongly influences the device conductance in zero and finite applied magnetic fields. Quantum dots with a sizable BR effect (i.e., with asymmetric spin-orbit scattering time shorter than the cavity dwell time) were found to display robust WAL signals with fluctuations consistent with the circular-symplectic ensemble.

A.L.R.B. and J.G.G.S.R. were supported by Conselho Nacional de Desenvolvimento Científico e Tecnológico (CNPq) Grant No. 307474/2018-6 and Fundação de Amparo à Ciência e Tecnologia do Estado de Pernambuco (FACEPE) Grant No. APQ-0325-1.05/18 (FACEPE). A.F. gratefully acknowledges the financial support from the Royal Society through a Royal Society University Research Fellowship.

[1] A. Avsar, H. Ochoa, F. Guinea, B. Özyilmaz, B. J. van Wees, and I. J. Vera-Marun, Rev. Mod. Phys. **92**, 021003 (2020).

[2] J. H. Garcia, M. Vila, A. W. Cummings, and S. Roche, Chem. Soc. Rev. **47**, 3359 (2018).

[3] M. Offidani and A. Ferreira, Phys. Rev. Lett. **121**, 126802 (2018).

[4] D. V. Tuan, F. Ortmann, D. Soriano, S. O. Valenzuela, and S. Roche, Nat. Phys. **10**, 857 (2014).

[5] C. L. Kane and E. J. Mele, Phys. Rev. Lett. **95**, 226801 (2005).

[6] C. L. Kane and E. J. Mele, Phys. Rev. Lett. **95**, 146802 (2005).

[7] F. J. Santos, D. A. Bahamon, R. B. Muniz, K. McKenna, E. V. Castro, J. Lischner, and A. Ferreira, Phys. Rev. B **98**, 081407(R) (2018).

[8] S. Wu, V. Fatemi, Q. D. Gibson, K. Watanabe, T. Taniguchi, R. J. Cava, and P. Jarillo-Herrero, Science **359**, 76 (2018).

[9] T. Frank, P. Högl, M. Gmitra, D. Kochan, and J. Fabian, Phys. Rev. Lett. **120**, 156402 (2018).

[10] J. Sichau, M. Prada, T. Anlauf, T. J. Lyon, B. Bosnjak, L. Tiemann, and R. H. Blick, Phys. Rev. Lett. **122**, 046403 (2019).

[11] J. O. Island, X. Cui, C. Lewandowski, J. Y. Khoo, E. M. Spanton, H. Zhou, D. Rhodes, J. C. Hone, T. Taniguchi, K. Watanabe, L. S. Levitov, M. P. Zaletel, and A. F. Young, Nature (London) **571**, 85 (2019).

[12] M. Offidani, M. Milletarì, R. Raimondi, and A. Ferreira, Phys. Rev. Lett. **119**, 196801 (2017).

[13] C. K. Safeer, J. Ingla-Aynés, F. Herling, J. H. Garcia, M. Vila, N. Ontoso, M. R. Calvo, S. Roche, L. E. Hueso, and F. Casanova, Nano Lett. **19**, 1074 (2019).

[14] T. S. Ghiasi, A. A. Kaverzin, P. J. Blah, and B. J. van Wees, Nano Lett. **19**, 5959 (2019).

[15] L. A. Benítez, W. Savero Torres, J. F. Sierra, M. Timmermans, J. H. Garcia, S. Roche, M. V. Costache, and S. O. Valenzuela, Nat. Mater. **19**, 170 (2020).

[16] L. Li, J. Zhang, G. Myeong, W. Shin, H. Lim, B. Kim, S. Kim, T. Jin, S. Cavill, B. S. Kim, C. Kim, J. Lischner, A. Ferreira, and S. Cho, ACS Nano **14**, 5251 (2020).

[17] D. Khokhriakov, A. M. Hoque, B. Karpiak, and S. P. Dash, Nat. Commun. **11**, 3657 (2020).

[18] S. A. Cavill, C. Huang, M. Offidani, Y.-H. Lin, M. A. Cazalilla, and A. Ferreira, Phys. Rev. Lett. **124**, 236803 (2020).

[19] Z. Wang, D.-K. Ki, J. Y. Khoo, D. Mauro, H. Berger, L. S. Levitov, and A. F. Morpurgo, Phys. Rev. X **6**, 041020 (2016).

[20] B. Yang, M.-F. Tu, J. Kim, Y. Wu, H. Wang, J. Alicea, R. Wu, M. Bockrath, and J. Shi, 2D Mater. **3**, 031012 (2016).

[21] B. Yang, M. Lohmann, D. Barroso, I. Liao, Z. Lin, Y. Liu, L. Bartels, K. Watanabe, T. Taniguchi, and J. Shi, Phys. Rev. B **96**, 041409(R) (2017).

[22] T. Völkl, T. Rockinger, M. Drienovsky, K. Watanabe, T. Taniguchi, D. Weiss, and J. Eroms, Phys. Rev. B **96**, 125405 (2017).

[23] S. Zihlmann, A. W. Cummings, J. H. Garcia, M. Kedves, K. Watanabe, T. Taniguchi, C. Schönenberger, and P. Makk, Phys. Rev. B **97**, 075434 (2018).

[24] T. Wakamura, F. Reale, P. Palczynski, S. Guéron, C. Mattevi, and H. Bouchiat, Phys. Rev. Lett. **120**, 106802 (2018).

[25] S. Hikami, A. I. Larkin, and Y. Nagaoka, Prog. Theor. Phys. **63**, 707 (1980).

[26] W. Knap, C. Skierbiszewski, A. Zduniak, E. Litwin-Staszewska, D. Bertho, F. Kobbi, J. L. Robert, G. E. Pikus, F. G. Pikus, S. V. Iordanskii, V. Mosser, K. Zekentes, and Yu. B. Lyanda-Geller, Phys. Rev. B **53**, 3912 (1996).

[27] E. McCann and V. I. Fal'ko, Phys. Rev. Lett. **108**, 166606 (2012).

[28] H. Liu, E. Marcellina, A. R. Hamilton, and D. Culcer, Phys. Rev. Lett. **121**, 087701 (2018).

[29] D. C. Marinescu, P. J. Weigele, D. M. Zumbühl, and J. C. Egues, Phys. Rev. Lett. **122**, 156601 (2019).

[30] S. Ilić, J. S. Meyer, and M. Houzet, Phys. Rev. B **99**, 205407 (2019).

[31] Z. Wang, D. Ki, H. Chen, H. Berger, A. H. MacDonald, and A. F. Morpurgo, Nature Comm. **6**, 8339 (2015).

[32] M. Gmitra, D. Kochan, P. Högl, and J. Fabian, Phys. Rev. B **93**, 155104 (2016).

[33] D. Kochan, S. Irmer, and J. Fabian, Phys. Rev. B **95**, 165415 (2017).

[34] T. P. Cysne, A. Ferreira, and T. G. Rappoport, Phys. Rev. B **98**, 045407 (2018).

[35] Additional SOCs are possible if low-symmetry transition metal dichalcogenides are used [34].

[36] L. A. Benítez, J. F. Sierra, W. Savero Torres, A. Arrighi, F. Bonell, M. V. Costache, and S. O. Valenzuela, Nat. Phys. **14**, 303 (2018).

[37] J. Xu, T. Zhu, Y. K. Luo, Y.-M. Lu, and R. K. Kawakami, Phys. Rev. Lett. **121**, 127703 (2018).

[38] J. C. Leutenantsmeyer, J. Ingla-Aynés, J. Fabian, and B. J. van Wees, Phys. Rev. Lett. **121**, 127702 (2018).

[39] S. Omar, B. N. Madhushankar, and B. J. van Wees, Phys. Rev. B **100**, 155415 (2019).

[40] C. W. J. Beenakker, Rev. Mod. Phys. **69**, 731 (1997).

[41] H. A. Weidenmüller and G. E. Mitchell, Rev. Mod. Phys. **81**, 539 (2009).

[42] C. W. J. Beenakker, *The Oxford Handbook of Random Matrix Theory* (Oxford University Press, Oxford, 2011), pp. 723–758.

[43] G. E. Mitchell, A. Richter, and H. A. Weidenmüller, Rev. Mod. Phys. **82**, 2845 (2010).

[44] I. L. Aleiner and V. I. Fal'ko, Phys. Rev. Lett. **87**, 256801 (2001).

[45] P. W. Brouwer, J. N. H. J. Cremers, and B. I. Halperin, Phys. Rev. B **65**, 081302(R) (2002).

[46] M. S. M. Barros, I. R. A. C. Lucena, A. F. M. R. Silva, A. L. R. Barbosa, and J. G. G. S. Ramos, Phys. Rev. B **99**, 195131 (2019).

[47] J. G. G. S. Ramos, A. L. R. Barbosa, and A. M. S. Macêdo, Phys. Rev. B **84**, 035453 (2011).

[48] R. A. Jalabert, H. U. Baranger, and A. D. Stone, Phys. Rev. Lett. **65**, 2442 (1990).

[49] A. Altland and M. R. Zirnbauer, Phys. Rev. B **55**, 1142 (1997).

[50] J.-H. Cremers, P. W. Brouwer, and V. I. Fal'ko, Phys. Rev. B **68**, 125329 (2003).

[51] D.-H. Choe and K. J. Chang, Sci. Rep. **5**, 10997 (2015).

[52] T. C. Vasconcelos, J. G. G. S. Ramos, and A. L. R. Barbosa, Phys. Rev. B **93**, 115120 (2016).

[53] J. G. G. S. Ramos, M. S. Hussein, and A. L. R. Barbosa, Phys. Rev. B **93**, 125136 (2016).

[54] J. Wurm, A. Rycerz, I. Adagideli, M. Wimmer, K. Richter, and H. U. Baranger, Phys. Rev. Lett. **102**, 056806 (2009).

[55] J. Wurm, K. Richter, and I. Adagideli, Phys. Rev. B **84**, 205421 (2011).

[56] F. Libisch, C. Stampfer, and J. Burgdörfer, Phys. Rev. B **79**, 115423 (2009).

[57] E. I. Rashba, Phys. Rev. B **79**, 161409(R) (2009).

[58] See Supplemental Material at http://link.aps.org/supplemental/10.1103/PhysRevB.103.L081111 for an introduction to the stub model and derivation of Eqs. (4) and (5) (given in Sec. S1 of the SM), for additional simulations of the conductance as a function of Fermi energy (given in Sec. S2 of the SM), and for estimation of mean level spacing, dwell time, and spin-orbit scattering time (given in Supplemental Table I of the SM).

[59] Y. Li and M. Koshino, Phys. Rev. B **99**, 075438 (2019).

[60] A. David, P. Rakyta, A. Kormányos, and G. Burkard, Phys. Rev. B **100**, 085412 (2019).

[61] This was first noted by McCann and Fal'ko within the context of diffusive (nonchaotic) quantum transport [27].

[62] T. P. Cysne, J. H. Garcia, A. R. Rocha, and T. G. Rappoport, Phys. Rev. B **97**, 085413 (2018).

[63] C. H. Lewenkopf and E. R. Mucciolo, J. Comput. Electron. **12**, 203 (2013).

[64] T. Verçosa, Y.-J. Doh, J. G. G. S. Ramos, and A. L. R. Barbosa, Phys. Rev. B **98**, 155407 (2018).

[65] F. A. F. Santana, J. M. da Silva, T. C. Vasconcelos, J. G. G. S. Ramos, and A. L. R. Barbosa, Phys. Rev. B **102**, 041107(R) (2020).

[66] C. W. Groth, M. Wimmer, A. R. Akhmerov, and X. Waintal, New J. Phys. **16**, 063065 (2014).

[67] H. U. Baranger, R. A. Jalabert, and A. D. Stone, Phys. Rev. Lett. **70**, 3876 (1993).

[68] L. A. Ponomarenko, F. Schedin, M. I. Katsnelson, R. Yang, E. W. Hill, K. S. Novoselov, and A. K. Geim, Science **320**, 356 (2008).

[69] C. Stampfer, E. Schurtenberger, F. Molitor, J. Güttinger, T. Ihn, and K. Ensslin, Nano Lett. **8**, 2378 (2008).

[70] K. Todd, H.-T. Chou, S. Amasha, and D. Goldhaber-Gordon, Nano Lett. **9**, 416 (2009).

[71] J. Güttinger, F. Molitor, C. Stampfer, S. Schnez, A. Jacobsen, S. Dröscher, T. Ihn, and K. Ensslin, Rep. Prog. Phys. **75**, 126502 (2012).